SCIENTIFIC REPORTS
nature research

OPEN

One-step Synthesized Silver Nanoparticles Using Isoimperatorin: Evaluation of Photocatalytic, and Electrochemical Activities

Maryamosadat Mavaei[1,4], Azam Chahardoli[1,4], Yalda Shokoohinia[1,2,4], Alireza Khoshroo[1] & Ali Fattahi[3*]

In the current study, isoimperatorin, a natural furanocoumarin, is used as a reducing reagent to synthesize isoimperatorin mediated silver nanoparticles (Iso-AgNPs), and photocatalytic and electrocatalytic activities of Iso-AgNPs are evaluated. Iso-AgNPs consisted of spherically shaped particles with a size range of 79–200 nm and showed catalytic activity for the degradation (in high yields) of New Fuchsine (NF), Methylene Blue (MB), Erythrosine B (ER) and 4-chlorophenol (4-CP) under sunlight irradiation. Based on obtained results, Iso-AgNPs exhibited 96.5%, 96.0%, 92%, and 95% degradation rates for MB, NF, ER, and 4-CP, respectively. The electrochemical performance showed that the as-prepared Iso-AgNPs exhibited excellent electrocatalytic activity toward hydrogen peroxide (H_2O_2) reduction. It is worth noticing that the Iso-AgNPs were used as electrode materials without any binder. The sensor-based on binder-free Iso-AgNPs showed linearity from 0.1 µM to 4 mM with a detection limit of 0.036 µM for H_2O_2. This binder-free and straightforward strategy for electrode preparation by silver nanoparticles may provide an alternative technique for the development of other nanomaterials based on isoimperatorin under green conditions. Altogether, the application of isoimpratorin in the synthesis of nano-metallic electro and photocatalysts, especially silver nanoparticles, is a simple, cost-effective and efficient approach.

Recently, isolated and purified natural products have gained considerable attention in the synthesis and cap of metallic nanoparticles. These natural product-induced metallic nanoparticles (NPIMNPs) have been widely used in the biological, environmental, electrochemical, and catalytic fields[1–8]. Albeit plant extracts are considered as general sources for the green synthesis of metallic nanoparticles[9], the extracts compositions and concentrations of substances are highly variable, affected by the method of extraction, harvesting season and geographical parameters. As an alternative, the pure natural products with a well–defined concentration of reactant can synthesize reproducible metallic nanoparticles, and the purification of nanoparticles is more facile[10,11].

Furthermore, physicochemical and biological characteristics of natural products can improve the biological, electrochemical, and catalytic properties of NPIMNPs. In this regard, natural products e.g., phenolic compounds, alkaloids, terpenoids, amino acids, flavonoids, glutathiones, quinones antioxidants, polysaccharides, organic acids, and coumarins have been used[12]. The synthesis of nanoparticles by these natural products is a clean, non-toxic, and environmental-friendly[13]. Compared to their counterparts, synthesized by other methods, NPIMNPs possess improved bioactivities and catalytic characteristics[12].

Among metallic nanoparticles, silver nanoparticles have been widely studied for catalytic activities. AgNPs can demonstrate light absorption and significant visible light catalytic activity due to its narrow bandgap energy

[1]Pharmaceutical Sciences Research Center, Health Institute, Kermanshah University of Medical Sciences, Kermanshah, Iran. [2]Ric Scalzo Botanical Research Institute, Southwest College of Naturopathic Medicine, Tempe, AZ, USA. [3]Medical Biology Research Center, Health Technology Institute, Kermanshah University of Medical Sciences, Kermanshah, Iran. [4]These authors contributed equally: Maryamosadat Mavaei, Azam Chahardoli and Yalda Shokoohinia. *email: a.fatahi.a@gmail.com

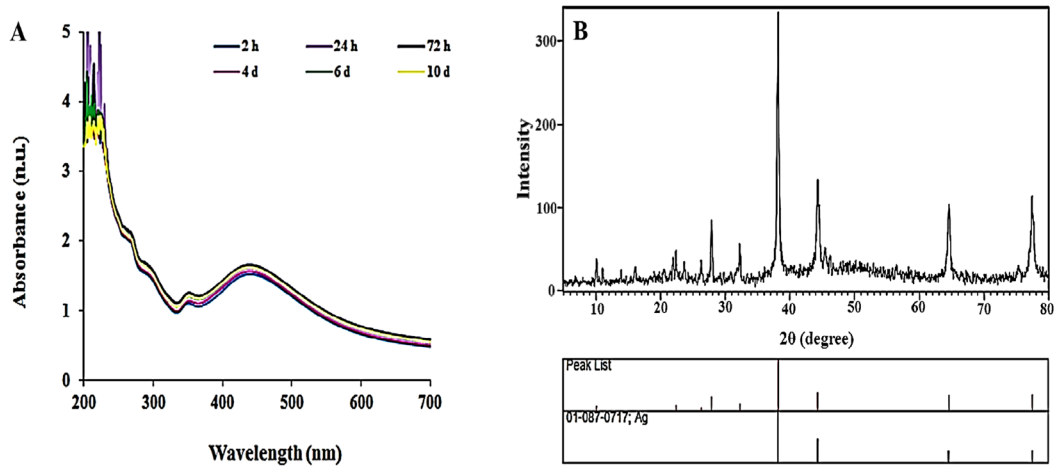

Figure 1. (**A**) UV–visible spectra at different intervals time and (**B**) XRD spectrum of Iso-AgNPs.

to the many colorant/textile combinations under visible or sunlight illumination[4,14]. The high absorption property of Ag-based NPs in the visible light region, together with preventing the recombination of electron and hole pairs within the photocatalytic process, drew enormous attention in the application of silver nanoparticles for the catalytic field. This aspect of AgNPs makes them an excellent choice for multiple roles in the industrial area[14]. Furthermore, AgNPs have been demonstrated to be good and impressible catalysts for non-enzymatic electrochemical detection of H_2O_2[15–20]. A large number of nanostructures decorated with chemically-stabilized AgNPs have been synthesized and used for this porpose[21].

Current techniques for the synthesis of AgNPs, including photochemical methods, chemical reduction, electron irradiation, gamma irradiation, and laser ablation[22], are expensive and require high temperature and pressure. Besides, they need toxic and hazardous chemicals like dimethylhydrazine, hydrazine and sodium borohydride and produce toxic organic byproducts that are responsible for various biological risks[23].

In addition to the synthesis limitations, the stabilization of AgNPs on the electrode surface hampered its application in the field of electrochemistry. In most of the cases, investigators used nonconductive polymers such as Nafion and chitosan as a binder[24–26]. Composites formed with nonconductive binders suffer from their low conductivity, which effects on the electrochemical response of nanocomposite-modified electrode, especially in traces analysis[27,28]. It is expected that the nonconductive materials can decrease the electrochemical performance of the nanomaterials. Therefore, the as-prepared binder-free electrode materials as stable catalysts with high conductivity and active surface area are highly demanded.

To address these unmet technical needs, in the present study, isoimperatorin was applied as a bio-reducing agent; photocatalytic and electrochemical activates of Iso-AgNPs were evaluated. Isoimperatorin is a furanocoumarin isolated from edible Apiaceous plants such as *Angelica dahurica*[29] and *Prangos ferulacea*[30]. It showed anti-inflammatory, anti-Alzheimer, analgesic, spasmolytic[31,32], potential cancer prevention[33], antibacterial and anti-cancer effects[34–37]. There are no reports on photo- or electrochemical-catalytic activities of isoimperatorin. However, there are some reports on electro-catalytic activities of other coumarins as chemo-sensors for the detection of fluoride ions, hydrogen sulfide (H_2S), mercury (Hg^{2+}) ions, hypochlorite, and cyanide anions in aqueous solution[38–42].

Although the different flavonoids, e.g. hesperidin, naringin, diosmin, quercetin diphosphate, and quercetin pentaphosphate, resveratrol and fisetin have been applied for the synthesis of AgNPs, and catalytic activity of synthesized NPs have been investigated[43,44], to our best of knowledge, there is no report on the synthesis of silver nanoparticles using isoimperatorin and evaluation of their catalytic properties. Therefore, in this work, we synthesized and characterized Iso-AgNPs using UV–visible spectrophotometer, Fourier-transform infrared spectroscopy (FTIR), scanning electron microscopy (SEM) with energy dispersive X-Ray (EDX) detector X-ray diffraction (XRD), Raman spectroscopy, transmission electron microscopy (TEM) and high-resolution transmission electron microscopy (HRTEM). The electrocatalytic activity of Iso-AgNPs toward H_2O_2 reduction and their photocatalytic performance against three toxic mutagenic dye pollutants consist of New-fuchsine (NF), Methylene Blue (MB) and Erythrosine B (ER), and 4-chlorophenol (4-CP) as a non-dye pollutant were evaluated.

Results and Discussion

Physical and chemical characterization of Iso-AgNPs. The reduction of the Ag^+ to AgNPs using isoimperatorin was approved by a color change from pale pink to dark brown after two h exposure; the absorption of Iso-AgNPs was shown in Fig. 1. The formation of dark brown color in the reaction mixture, indicating the excitation of Surface Plasmon Resonance (SPR) of Iso-AgNPs is a sign for the synthesis of AgNPs[45,46]. Iso-AgNPs showed a clear and single SPR band with λ_{max} (maximum absorption) at 439 nm (Fig. 1A).

Iso-AgNPs had a face-centered cubic crystalline nature according to the XRD pattern (Fig. 1B). Four reflection peaks were detected in the 2θ range of 20–80°; peaks at 38.1, 44, 64.3, and 77.3° are allocated to the (111), (200), (220), and (311) planes for Iso-AgNPs respectively. The extra picks presented in the spectrum can belong to isoimperatorin[47].

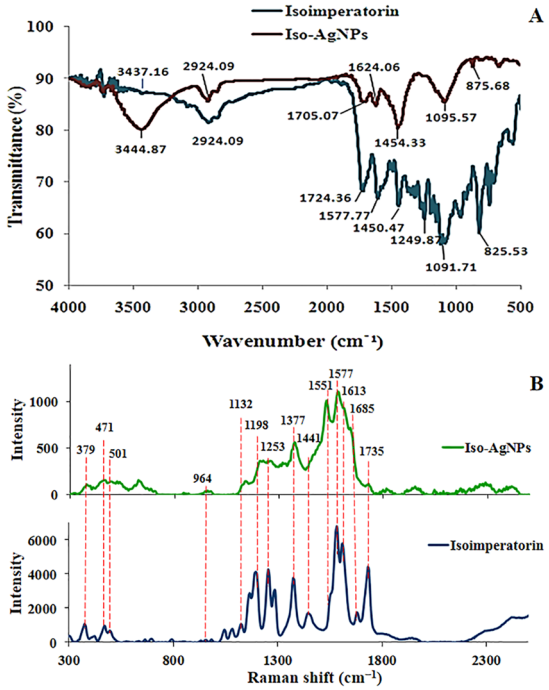

Figure 2. (**A**) FTIR and (**B**) Raman spectra of isoimperatorin and Iso-AgNPs.

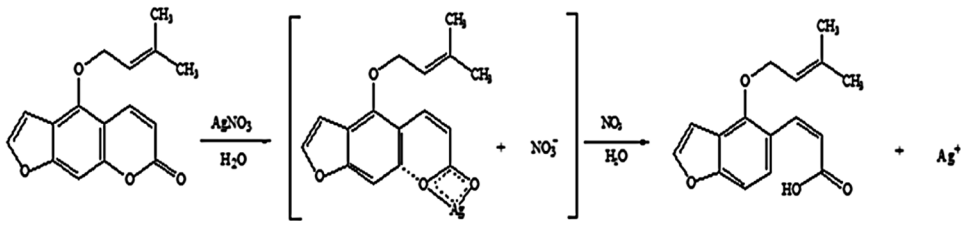

Figure 3. The possible reaction of $AgNO_3$ with isoimperatorin.

The possible changes in the structure of isoimperatorin after synthesis of AgNPs were evaluated by FTIR. The FTIR spectra of pure isoimpratorin and synthesized AgNPs are shown in Fig. 2A. Comparing to the isoimperatorin spectrum, some functional groups were disappeared, and new peaks appeared in the FTIR spectrum of Iso-AgNPs. The FTIR spectrum of isoimperatorin indicated the characteristic peak at 1724 cm^{-1} related to stretching vibrations of carbonyl bands from ester group, and the peak at 1249 and 1091 cm^{-1} corresponding to -C-O- of ester group, but the Iso-AgNPs spectrum showed the peak at 1705 cm^{-1} related to stretching vibrations of carbonyl bands from carboxylic acid group, and the peak at 1095 cm^{-1} attributed to C-O- stretching vibration of carboxylic acid group. Also, the broad peak of the OH group at 3444 cm^{-1} was appeared affirming the presence of the carboxylic acid group. Due to the presence of Ag^+ ions in the stereochemical medium, carboxylate anion is formed, and then carboxylate anion becomes carboxylic acid by the catalytic effect of nitric acid (the byproduct of carboxylate anion). The possible reaction of $AgNO_3$ with isoimperatorin is illustrated in Fig. 3. For further characterization of Iso-AgNPs, Raman spectroscopy data has been provided. In Fig. 2B, the Raman spectrum of isoimperatorin, is compared with the spectra of Iso-AgNPs. Characteristic peaks (1685, 1613, 1577, 1551, 1441, 1377, 1253, 1198, 1132, 964, 501, 471, and 379 cm^{-1}) from Iso-AgNPs were attributed to isoimperatorin[10,48]. The result indicates that the isoimperatorin is mainly involved in the fabrication of silver nanoparticles. Based on the proposed mechanism for the reaction of $AgNO_3$ with isoimperatorin (Fig. 3), the C=O function related to the ester group converts to the carboxylic acid group; therefore, C=O stretching in the Raman spectrum of pure isoimperatorin (1735 cm^{-1}) was abolished. These results confirm FTIR results.

The SEM analysis showed well defined uniformly spherical Iso-AgNPs without any agglomeration and their small size (Fig. 4A). EDX analysis confirmed the presence of elemental silver in the sample (Fig. 4B). The sharp peak at 3.030 keV represented the existence of elemental silver.

The morphology and particle size of Iso-AgNPs were evaluated by TEM image (Fig. 5A); nanoparticles were spherical in shapes. The spherical nanostructure had a diameter range of 79–200 nm. The presence of large particles can be related to slow reaction speed[49,50]. Isoimperatorin solubility in water is low, and using a high

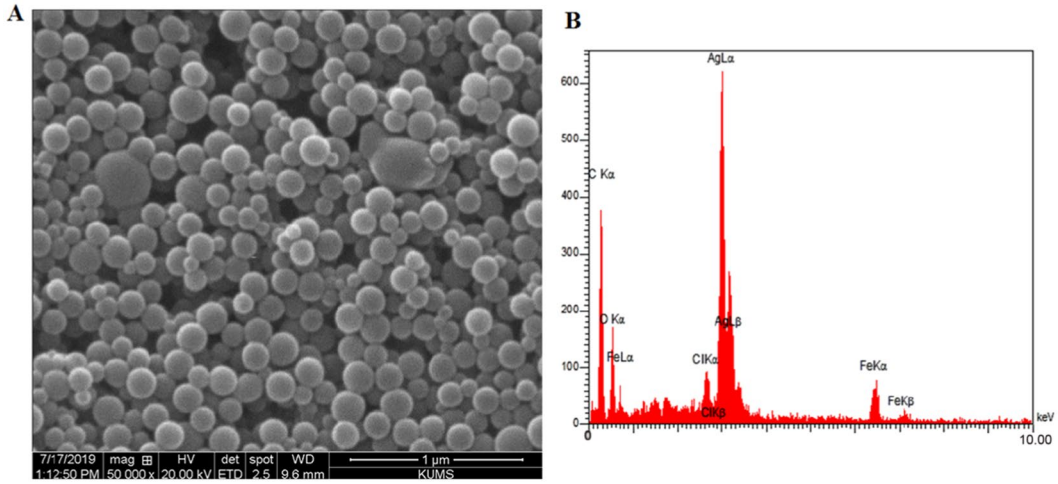

Figure 4. (**A**) SEM micrographs and (**B**) EDX spectra of Iso-AgNPs.

concentration of it in the aqueous medium is impossible. Therefore, the rate of nucleation was low, and crystals had enough time for growth.

Figure 5B shows the HRTEM image of the Iso-AgNPs. In inset Fig. 5B, the interplanar distance of 2.21°A can be observed. The crystallinity of Iso-AgNPs was observed by selected area emission diffraction (SAED), which recorded by directing the electron beam perpendicular to NPs. The characteristic fringe array can be indexed as (111), (200), (220) and (311) of the pure face-centered cubic (fcc) lattice structure commonly found for Ag crystal (Fig. 5C). The formation of fcc structured Iso-AgNPs was also confirmed using the XRD patterns.

Photo-catalytic performance of Iso-AgNPs. The photocatalytic activity of Iso-AgNPs was analyzed by photo-degradation of NF, MB, ER dyes as a model. As shown in Fig. 6, the degradation of tree dyes under sunlight irradiation initially identified by the color change into light color and then colorless after 60 min for MB, ER, and NF dyes. The UV–vis absorption spectra indicated the decreased peaks for three studied dyes at different time intervals. Initially, the sharp decline occurred for absorption peaks at 548 nm for NF (Fig. 6A), 665 nm for MB (Fig. 6B), and 526 for ER (Fig. 6C) at 15 min under sunlight irradiation. It was continued with the increase of the exposure time. The degradation rates of MB, ER, and NF dyes were 96.5%, 92%, and 96.0%, respectively, at 60 min (Fig. 7A).

In order to examine the reusability and durability of as prepared Iso-AgNPs photocatalyst, a recycling study of Iso-AgNPs was carried out with a stock solution of NF (as a dye molecule model for this section) under identical conditions. Hence, the stability of the Iso-AgNPs was tested for successive four recycling runs. As shown in Fig. 7B, the reusability of the Iso-AgNPs photocatalyst was demonstrated up to a fourth cycle run with a low decrease in photo-degradation efficiency, i.e., 96% to about 88% in the first to fourth cycle runs. The results presented in Fig. 7B demonstrate that the Iso-AgNPs possess robust and excellent cycle stability.

Possible photo-catalytic mechanism of Iso-AgNPs. The photocatalytic reaction on the surface of the catalyst generally involves the absorption of light, generation of charge carriers, transport of electron and hole pairs (e^-_{CB}/h^+_{VB}) and surface oxidation-reduction processes. The light from the sunlight irradiation can be absorbed efficiently by both the catalyst and the dye molecules. On irradiation by a photon, Iso-AgNPs absorb the photons with an energy $h\nu$ and due to their high SPR effect subsequently, generate electrons (e^-_{CB}) and holes (h^+_{VB}) pair (Eq. 1)[51]. The dye molecule can also act as a photosensitizer[52–54] and it was adsorbed on catalyst surface during the oxidation-reduction experiment (Eqs. 2 and 3). The adsorbed dye molecule (i.e., NF, ER, and MB) was excited by absorbing light and donates its photo-generated electron to the conduction band (CB) of Iso-AgNPs. The photo-generated electrons reduce molecular oxygen (O_2) adsorbed on the photo-catalyst surface into superoxide radical anions ($O_2^-\bullet$) and hydrogen peroxide radicals ($\bullet$OOH), quickly (Eqs. 4–7)[53,55]. The photo-generated holes could directly oxidize adsorbed dye molecules or react with surface adsorbed water molecules (H_2O) or hydroxyl (OH^-) to generate hydroxyl radicals (HO$\bullet$) (Eqs. 8, 9 and 10)[55]. As a result, active species (radicals) were generated and assist in the photo-degradation and mineralization of dye molecules (Eq. 11). The possible mechanism for the Iso-AgNPs photodegradation of dyes was proposed in Fig. 8.

$$\text{Iso} - \text{AgNPs} + \text{sunlight} \rightarrow \text{Iso} - \text{AgNPs}(e^-_{CB} + h^+_{VB}) \quad (1)$$

$$\text{Dye} + \text{sunlight} \rightarrow \text{Dye}^* \quad (2)$$

$$\text{Dye}^* + \text{Iso} - \text{AgNPs} \rightarrow \text{Dye}^{\cdot+} + \text{Iso} - \text{AgNPs}(e^-_{CB}) \quad (3)$$

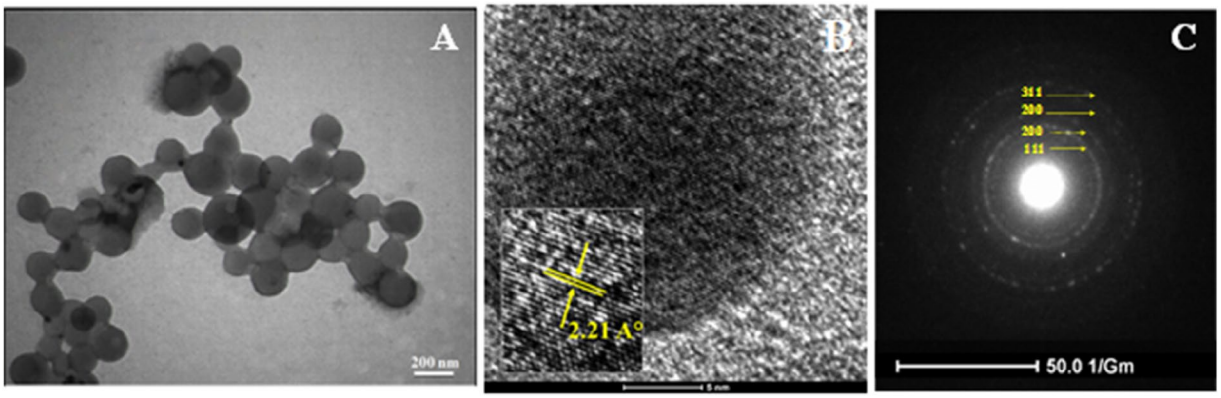

Figure 5. (**A**) TEM, (**B**) HRTEM and (**C**) SAED micrographs of Iso-AgNPs.

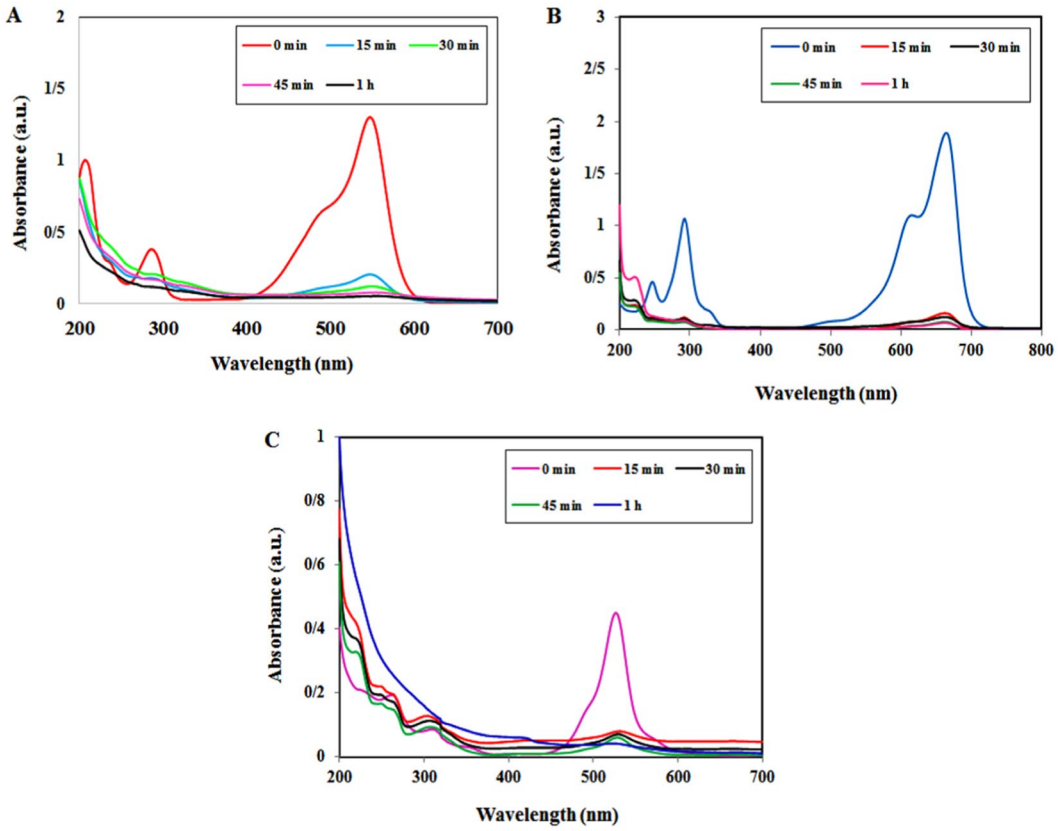

Figure 6. The photocatalytic activity of Iso-AgNPs. UV–vis spectra for photo-degradation of (**A**) NF, (**B**) MB and (**C**) ER Dyes under sun-light irradiation with the Iso-AgNPs.

$$(O_2) + \text{Iso} - \text{AgNPs}(e^-_{CB}) \rightarrow \text{Iso} - \text{AgNPs} + (O_2\cdot^-) \quad (4)$$

$$(O_2\cdot^-) + H^+ \rightarrow HO_2\cdot \quad (5)$$

$$2HO_2\cdot \rightarrow O_2 + H_2O_2 \quad (6)$$

$$H_2O_2 + (O_2\cdot^-) \rightarrow HO^- + HO\cdot + O_2 \quad (7)$$

$$e^- + H_2O_2 \rightarrow HO\cdot + HO^- \quad (8)$$

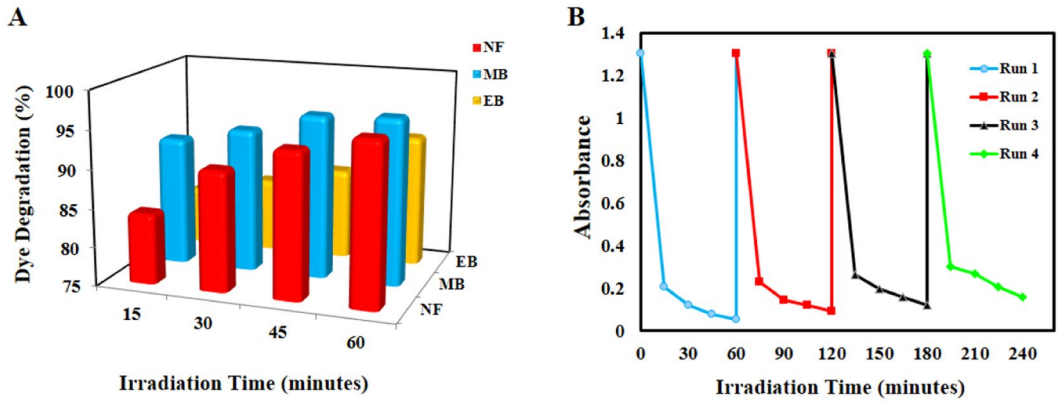

Figure 7. (**A**) The degradation rate (%) of NF, MB and ER dyes over the Iso-AgNPs photocatalyst. (**B**) Reusability of the Iso-AgNPs after four successive runs.

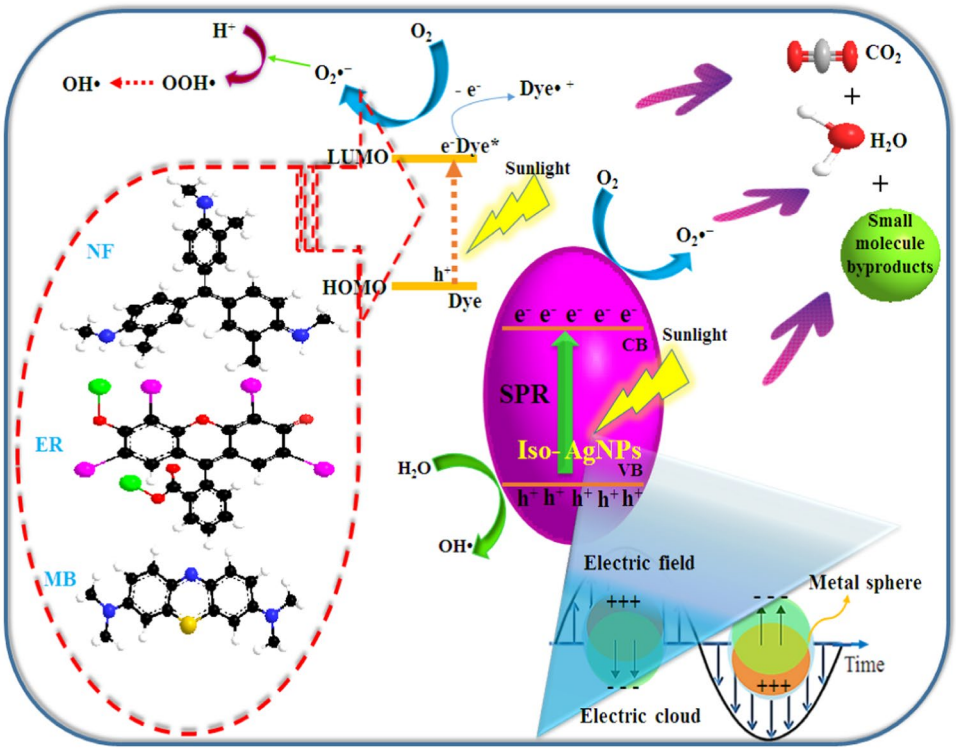

Figure 8. The photo-degradation pathway of dye pollutants in the presence of Iso-AgNPs under sunlight irradiation.

$$(H_2O) + \text{Iso} - \text{AgNPs}(h^+_{VB}) \rightarrow \text{Iso} - \text{AgNPs} + (HO\cdot) + (H^+) \quad (9)$$

$$(HO^-) + \text{Iso} - \text{AgNPs}(h^+_{VB}) \rightarrow \text{Iso} - \text{AgNPs} + (HO\cdot) \quad (10)$$

$$\text{Dye} + \text{Iso} - \text{AgNPs}(O_2\cdot^-, HO\cdot, h^+_{VB} \text{ or } \cdot OOH) \rightarrow \rightarrow \rightarrow H_2O + CO_2 + \text{byproducts} + \text{Free Iso} - \text{AgNPs for reuse} \quad (11)$$

For approving that the fading of dye is photo-degradation, not a dye sensitization, carcinogenic 4-chlorophenol (4-CP) as a colorless organic pollutant was selected as a target to measure the photocatalytic activity. The evolution of UV-vis spectra of carcinogenic 4-CP under natural sunlight in the presence of the Iso-AgNPs is presented in Fig. 9A; the intensities of peaks at 225 nm and 280 nm characteristic of 4-CP, was decreased in a function of difference irradiation times. Although many aspects regarding the detailed degradation mechanisms of the

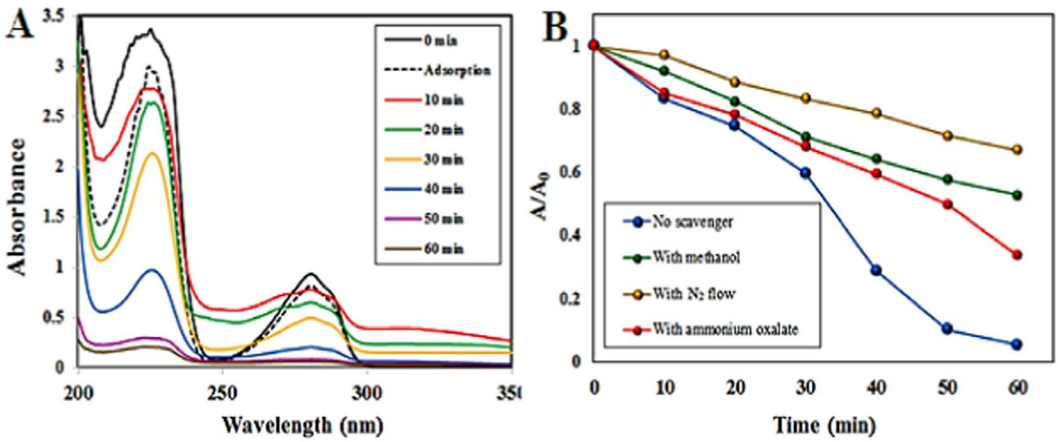

Figure 9. (**A**) UV-vis spectra of the aqueous solution of 40 ppm 4-CP in the presence of Iso-AgNPs photocatalyst. (**B**) The impact of different radical scavengers on the photocatalytic degradation of 4-CP by Iso-AgNPs under natural sunlight.

4-CP remain unidentified and open to further scrutiny, some primary degradation pathway includes a series of hydroxylation, dehydrogenation, dechlorination and aromatic ring cleavage steps[56–59]. According to the literature, decomposition of 4-CP to H_2O and CO_2 molecules as the final products often is a complex process occurring through three primary intermediates: benzoquinone (BQ), hydroquinone (HQ), and 4-chlorocatechol (4-CC)[60,61]. The characteristic absorption peaks of these compounds emerge as intermediates at similar wavelengths as those of 4-CP, i.e. at 246 nm for BQ, 221 nm and 290 nm for HQ, 221 and 284 nm for 4-CC[62]. As can be seen, a gradual decrease of both absorption peaks of 4-CP during photocatalytic procedure may be an indication of decomposition of 4-CP. On the other hand, the lack of the absorption peak characteristic of BQ intermediates at 246 nm in the spectra observed in Fig. 9A suggests that reaction pathway in the presence of Iso-AgNPs is via 4-CC intermediate[62].

As shown in Fig. 9A, prior to the photocatalytic tests, the adsorption of 4-CP was evaluated. However, the dark physical adsorption of the 4-CP after 60 min onto the nano-photocatalysts was negligible (point line, Fig. 9A) while in photocatalytic process, the decrease of the absorption band of 4-CP was quick. This notable decrease indicated that the removal was also mainly originated from the photocatalytic degradation, not from physical adsorption.

To well understand the presence and role of active species in the photocatalytic degradation route of the organic compounds, the scavenger quenching experiments for 4-CP photo-degradation was selected and carried out at 40 ppm 4-CP concentration for 60 min. Various scavengers used in the present study were ammonium oxalate as an H^+ scavenger, methanol as an HO• scavenger, and in deoxygenated solutions to conquer the formation of O_2^-• by oxygen reduction.

As indicated in Fig. 9B, by addition of oxalate, a slight inhibitory effect was found where around 66% of 4-CP was degraded under natural sunlight. Conversely, deoxygenation of the 4-CP solution significantly decreased the 4-CP molecule photocatalytic degradation rate, where only 34% of 4-CP is removed. Similarly, the existence of methanol leads to an impressive decrease in 4-CP degradation, where about 48% of 4-CP is degraded under natural sunlight. This suggests that the superoxide radicals and then hydroxyl radicals play an important role and acts as main reactive species in the pollutant photo-decomposition. The 4-CP decomposition efficiency was 95.0% without using any scavenger.

Electrochemical properties of Iso-AgNPs. The electrocatalytic activity of the Iso-AgNPs as a binder-free catalyst for H_2O_2 reduction was investigated by recording cyclic voltammograms in presence of the H_2O_2. Figure 10A shows the electrochemical reduction of 1.0 mM H_2O_2 at Iso-AgNPs/GCE (Glassy Carbon Electrode) in N_2-saturated 0.1 M PBS (pH 7.4) at the scan rate of 100 mV/s. As can be seen, at the unmodified GCE, there is no obvious current for the reduction of H_2O_2. However, the presence of Iso-AgNPs on the electrode surface had a great improvement on the electrocatalytic reduction of H_2O_2, which indicated that the Iso-AgNPs facilitate the electron transfer and increased active surface area. Furthermore, the binder-free Iso-AgNPs can further improve electrochemical performance and electron kinetics of H_2O_2 reduction. In the following, to investigate the sensitivity of Iso-AgNPs on the reduction of H_2O_2, the cyclic voltammograms were obtained at a different concentration of H_2O_2 in N_2-saturated 0.1 M PBS (pH 7.4), (Fig. 10B). As expected, the peak current increased with the increasing concentration of H_2O_2, indicating the catalytic activity of Iso-AgNPs to the reduction of H_2O_2. Also, the sensing stability of binder-free Iso-AgNPs was examined by successive cyclic voltammograms in the presence of H_2O_2. As shown in Fig. 10C, after 9 cycles, the reduction peak currents only varied ~6%, indicating that Iso-AgNPs has good stability on the electrode surface for electrochemical reduction of H_2O_2. Therefore, the as-prepared Iso-AgNPs could be used as an electrocatalyst without any binder and shows the acceptable stability on the electrode surface.

Differential pulse voltammetry (DPV) was used for the analytical performance of the electrochemical sensor based on Iso-AgNPs toward the reduction of H_2O_2. Figure 11 shows the DPV response of Iso-AgNPs/GCE

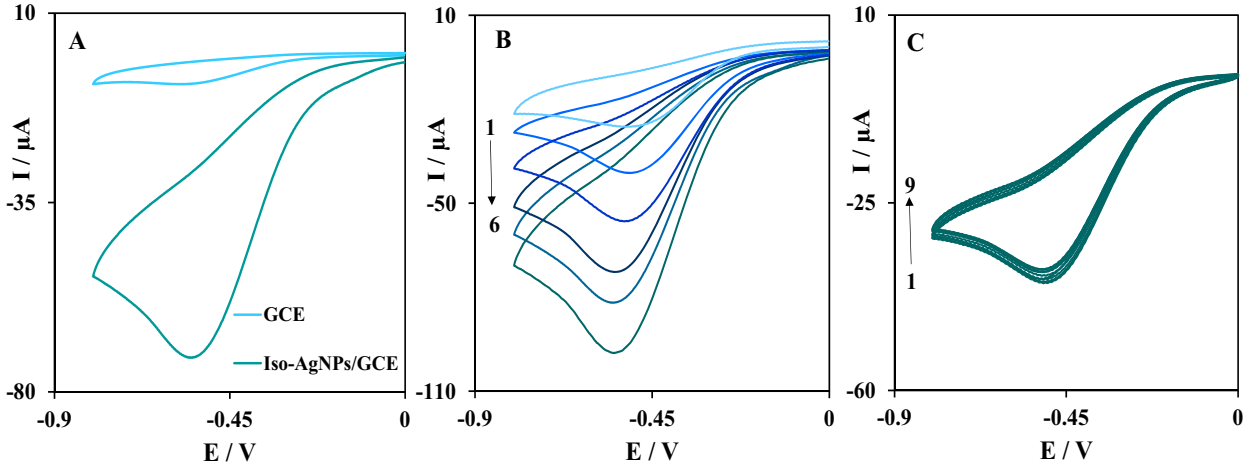

Figure 10. (**A**) Cyclic voltammograms of GCE and Iso-AgNPs/GCE in N_2-saturated 0.1 M PBS (pH 7.4) containing 1 mM H_2O_2 at a scan rate of 100 mV/s, (**B**) Cyclic voltammograms of Iso-AgNPs/GCE in the presence of various concentrations of H_2O_2 (peak No.1 to 6 correspondent to conc. 0.15, 0.3, 0.6, 1, 1.3 and 1.6 mM H_2O_2, respectively), (**C**) Repetitive cyclic voltammograms (peak No. 1 to 9) of Iso-AgNPs/GCE in the presence of H_2O_2.

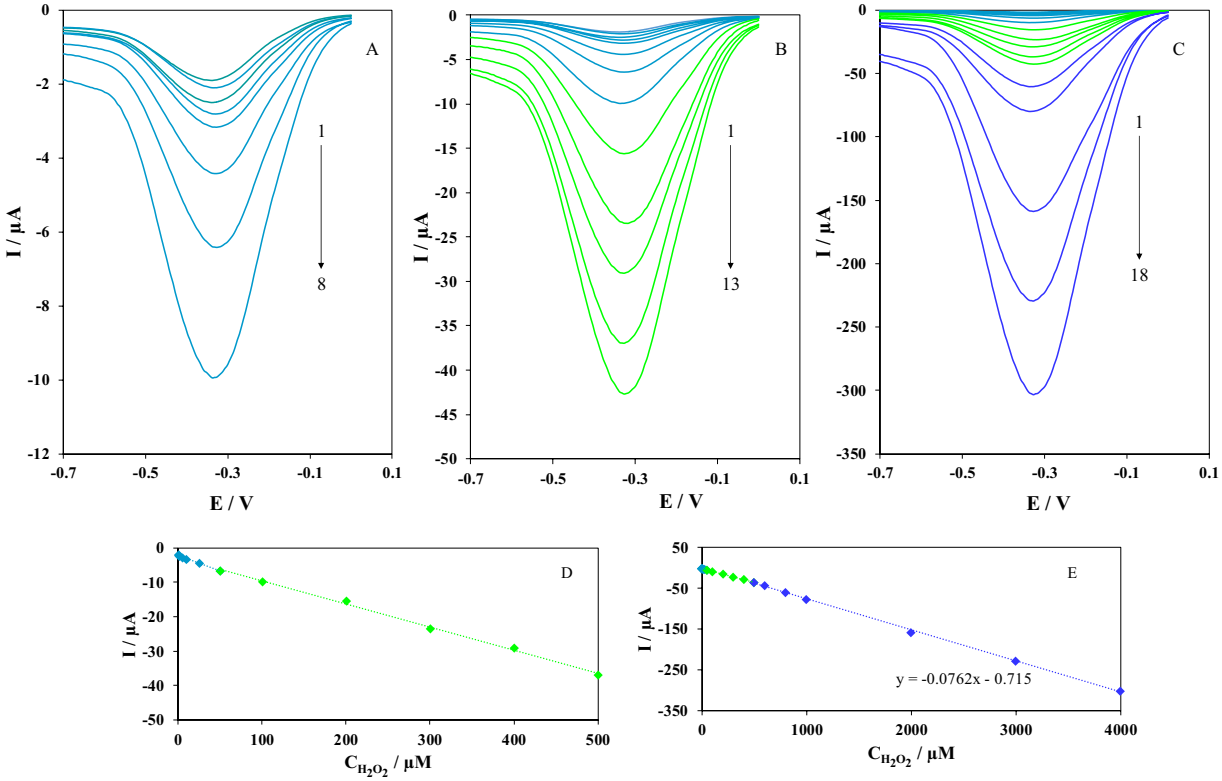

Figure 11. DPVs of Iso-AgNPs/GCE in N_2-saturated 0.1 M PBS (pH 7.4) containing different concentrations of H_2O_2; (**A**) Peak No. 1 to 8 correspondent to 0.1 to 50 µM of H_2O_2, (**B**) Peak No. 1 to 13 correspondent to 0.1–500 µM, (**C**) Peak No. 1 to 18 correspondent to 0.1–4000 µM, (**D**,**E**) Plot of the peak currents as a function of H_2O_2 concentration, peaks 1–13 and 1–18 respectively.

obtained at different H_2O_2 concentration in N_2-saturated 0.1 M PBS (pH 7.4). As expected, the response of Iso-AgNPs/GCE corresponding to the H_2O_2 increased with increasing the concentration of H_2O_2. The calibration curves of the H_2O_2 sensor showed that there was a linear relationship between the electrochemical responses and H_2O_2 concentrations from 0.1 µM to 4 mM. Based on the calibration curves in Fig. 11D,E, the plot of electrochemical responses vs. H_2O_2 concentration formed a line that had an equation of I (µA) = 0.0762 CH_2O_2 (µM) + 0.715. Furthermore, the limit of detection (LOD) was estimated as 0.036 µM from the calibration plot

Material of sensor	Linear range	LOD	Reference
Prussian Blue	0.01 μM – 10 mM	0.01 μM	[63]
Cobalt nitride nanowire array on Ti	0.1 μM – 2.5 mM	50 nM	[64]
Pt NPs-carbon quantum dots on GO	1 μM – 900 μM	0.1 μM	[65]
Gr supported intermetallic PtPb NPs	2 nM – 2.5 mM	2 nM	[66]
Silver nanowire	0.1 mM – 3.1 mM	29.2 μM	[67]
GO decorated with silver NPs	0.1 mM – 5 mM	1.099 μM	[68]
Ag@C@Ag trilaminar core-shell	70 μM – 10 mM	23 μM	[69]
Iridium (III) complex	8.0 pM – 2.0 nM	3.2 pM	[70]
Fe_3O_4 nanoparticles	4.18 μM – 0.8 mM	1.4 μM	[71]
Co metal-organic framework	5 μM – 9.0 mM	3.76 μM	[72]
Iso-AgNPs	0.1 μM – 4 mM	0.036 μM	This work

Table 1. A comparison with other sensors for the detection of H_2O_2.

with a signal-to-noise ratio of 3. The results of the proposed electrochemical sensor based on Iso-AgNPs are comparable with other modified electrode for H_2O_2 sensing and are displayed in Table 1[63–72]. However, our electrochemical sensor is characterized by a binder-free, simple design and easy preparation in contrast with other sensors previously described.

Conclusion

Isoimperatorin, isolated from *Prangos ferulacea* roots, was used successfully to synthesize silver nanoparticles as a simple and cost-effective, precise and eco-friendly methodology. Preparation of Iso-AgNPs was confirmed by UV–Vis spectroscopy and characterization was conducted using XRD, FTIR, SEM, EDX, Raman spectroscopy, TEM and HRTEM. The Iso-AgNPs reveal photo-catalytic performance under sunlight irradiation and can be used for the improvement of the environment through the purification of water. Also, Iso-AgNPs shows the excellent electrocatalytic activity toward H_2O_2 as an appropriate option in many biological systems without extra binder and conductive additives. Altogether, the synthesized nanoparticles demonstrate a broad range of catalytic applications.

Materials and Methods

Materials. Silver nitrate salt ($AgNO_3$), MB, NF, EB, 4-CP, ammonium oxalate, methanol, heptane, ethyl acetate, and silica gel were bought from Merck, Germany. Deuterochloroform ($CDCl_3$) was supplied from Sigma–Aldrich, USA. Other reagents, solid materials, Silica gel used in gravity column chromatography and solvents were bought from Merck (Germany).

Experimental

Apparatus. A Young Lin apparatus equipped with PDA detector (YL 9160) and a binary pump (YL 9111 S) together with VERTISEP (Reversed-phase, RP18 250 × 30 mm) and Eurospher II (Normal phase, Si 250 × 20 mm) columns with flow rate of 10 mL/min have been used for high-performance liquid chromatography (HPLC) analysis.

The NMR spectrum of Isoimperatorin was recorded on a BRUCKER (500 MHz) instrument, using $CDCl_3$ as a solvent. MS analysis was performed on an AGILENT 6410 Triple Quadrupole mass spectrometer (AGILENT Technologies, Palo Alto, CA, USA)[73] coupled with an AGILENT Mass Hunter Workstation B.01.03. TLC plates (Silica gel 60 GF254 precoated plates, Merck) were analyzed by UV observation at 254 and 366 nm, and by spraying with cerium sulfate/ molybdate[74].

The synthesis of Iso-AgNPs was confirmed by UV–vis spectrometer (SHIMADZU, Lambda UV mini-1240 instrument) in the absorption wavelength range of 200 to 700 nm. The FTIR of isoimperatorin and Iso-AgNPs was performed by IR-Prestige-21 (SHIMADZU Spectrometer, Kyoto, Japan); KBr Pellets of samples were used to measure transmittance percentage. The spectrum was recorded at a resolution of 4 cm^{-1}. The XRD spectrum of the dried nanoparticles was recorded by APD 2000-Italian Structures X-ray generator; to carry out XRD, the samples were coated on the XRD grid, and a voltage of 40 kV with a current of 30 mA using Cu K^{-1} radiation was applied. The SEM and EDX (FESEM-TSCAN, Czech), were performed for the analysis of surface topographies and chemical composition of Iso-AgNPs. Raman spectroscopy was performed by NICOLET-910, USA. The morphological analysis of NPs was evaluated by TEM microscopy (ZEISS – EM10C, Germany) and HRTEM microscopy (FEI – TEC9G20, USA) at an accelerating voltage of 100 kV and 200 kV, respectively. The aqueous suspension of Iso-AgNPs was loaded on the carbon-coated copper grid. After evaporation of solvent at room temperature for one-hour, clear microscopic views were observed in the different range of magnifications. The light intensity in the place of the sample was gotten from Kermanshah weather bureau. Electrochemical studies were conducted with an AUTOLAB PGSTAT101 potentiostat/galvanostat (ECO CHEMIE, Netherlands) with standard three-electrode system, using GCE or a modified GCE as working electrode, a platinum wire as a counter electrode and Ag/AgCl/KCl as a reference electrode.

Isolation of isoimperatorin. Isoimperatorin was isolated from *Prangos ferulacea* roots as described previously[75]. In brief, a MeOH-soluble (in −20 °C) part of acetone extract of roots was fractionated using heptane ethyl acetate (7:3) as the eluant and silica gel as the stationary phase. The final purification was performed by normal phase preparative HPLC.

Isoimperatorin; EI-MS m/z 270 $[M]^+$, 255 [M-CH3], 227 [M-(CH3)2CH] $^+$.H^1NMR ($CDCl_3$, 500 MHz): 8.19 d (1 H, J: 9.6, H-4), 7.62 d (1 H, *J*: 2.3, H-2′), 7.19 s (1 H, H-8), 6.99 d (1 H, *J*: 2.3, H-3′), 6.30 d (1 H, *J*: 9.6, H-3), 5.75 t (1 H, *J*: 6.8, H-2″), 4.95 d (2 H, *J*: 6.8, H-1″), 1.84 s (3 H, CH3–5″), 1.73 s (3 H, CH3–6″).

Synthesis of AgNPs with isoimperatorin. The isoimperatorin solution (2 mmol/L) was obtained by dissolving isoimperatorin in 2 mL ethanol. Then, the ethanol solution was added dropwise to 6 mL deionized water and incubated for 10 min at room temperature. Then, the isoimperatorin solution was quickly added to 12 mL aqueous solution of $AgNO_3$ (1 mmol/L). Finally, the reaction was placed under sunlight (The light intensity was 25.5 MJ/m^2) to change the color from pale yellow to reddish-brown which indicates the formation of Iso-AgNPs.

Photocatalytic properties of Iso-AgNPs. Using the four kinds of hazardous pollutant involve three dyes model (MB, NF, and ER) and carcinogenic 4-CP as a non-dye pollutant, the photocatalytic activity of Iso-AgNPs was demonstrated under sunlight irradiation by a slightly modified method of Roy *et al.*[76]. Primarily, the dye and non-dye solutions were prepared at a concentration of 10 mg/L and 40 mg/L in DI water respectively. Afterward, 5 mg of Iso-AgNPs was added to 25 mL of each dye solution (at first, powder of Iso-AgNPs was sonicated in 5 mL DI water for 15 min and then added to 20 mL pollutant solution). These colloidal suspensions were then placed under natural sunlight irradiation with constant stirring. The average temperature of the ambiance during the test was around 14 °C (geographical coordinates: 34.3277°N and 47.0778°E) and the light intensity was 7.7 MJ/m^2 for MB, NF, and ER. In the case of 4-CP, the average temperature was around 21 °C and the light intensity was 9.9 MJ/m^2. At regular intervals time (every 15 min for dye model and every 10 min for 4-CP), 2 mL suspension was taken from the colloidal mixture and centrifuged at 5,000 rpm for15 min to obtain clean supernatant of the tested pollutant. Finally, the absorbance maxima of dye models at different time intervals (0, 15, 30, 45, 60 min) was monitored using UV–visible spectrophotometer at a different wavelength from 200 to 800 nm for evaluation of dye degradation. The absorbance maxima of 4-CP were monitored at 0, 10, 20, 30, 40, 50 and 60 min time intervals.

Free radical trapping experiments. The scavenger quenching was investigated by adding scavengers consisting 0.5 mM methanol (a quencher of •OH), nitrogen (a quencher of $\bullet O_2^-$, 0.3 L/min), and 0.5 mM ammonium oxalate (a quencher of h^+) to evaluate the effect of each radical on the photo-degradation process of the pollutants.

Electrochemical measurement procedure. Iso-AgNPs modified GCE was constructed by the drop-casting method. Before modification, the working electrode was polished with alumina powder on a mirror-like surface. A volume of 5 µL of the Iso-AgNPs aqueous solution was applied directly on a cleaned GCE surface and drying at room temperature to obtain Iso-AgNPs/GCE. After modification, cyclic voltammetry and differential pulse voltammetry was used to characterize the electrocatalytic activity and stability of the Iso-AgNPs toward reduction of H_2O_2 in 0.1 M PBS (pH 7.4). The PBS buffer was purged with ultrapure nitrogen for 10 min to remove dissolved oxygen before the measurement.

Statistical analysis. One-way Analysis of Variance (ANOVA) and Tukey-Kramer post-test was applied for the determination of differences between groups at $p < 0.05$ level using SPSS statistical package (SPSS, Version 16 for Windows, SPSS Inc., Chicago, USA).

Received: 27 September 2019; Accepted: 23 December 2019;
Published online: 04 February 2020

References

1. Griffin, S. *et al.* Natural nanoparticles: A particular matter inspired by nature. *Antioxid.* **7**, 3 (2018).
2. Bhagat, M., Anand, R., Datt, R., Gupta, V. & Arya, S. Green Synthesis of Silver Nanoparticles Using Aqueous Extract of Rosa brunonii Lindl and Their Morphological, Biological and Photocatalytic Characterizations. *J. Inorg. Organomet. Polym. Mater.* **29**, 1039–1047 (2019).
3. Momin, B., Rahman, S., Jha, N. & Annapure, U. S. Valorization of mutant Bacillus licheniformis M09 supernatant for green synthesis of silver nanoparticles: photocatalytic dye degradation, antibacterial activity, and cytotoxicity. *Bioprocess. Biosyst. Eng.* **42**, 541–553 (2019).
4. Wang, F. *et al*. Extract of Ginkgo biloba leaves mediated biosynthesis of catalytically active and recyclable silver nanoparticles. *Colloids Surf. A: Physicochemical Eng. Asp.* **563**, 31–36 (2019).
5. Wang, L., Lu, F., Liu, Y., Wu, Y. & Wu, Z. Photocatalytic degradation of organic dyes and antimicrobial activity of silver nanoparticles fast synthesized by flavonoids fraction of Psidium guajava L. leaves. *J. Mol. Liq.* **263**, 187–192 (2018).
6. Kathiravan, V. Green synthesis of silver nanoparticles using different volumes of Trichodesma indicum leaf extract and their antibacterial and photocatalytic activities. *Res. Chem. Intermed.* **44**, 4999–5012 (2018).
7. Parthiban, E., Manivannan, N., Ramanibai, R. & Mathivanan, N. Green synthesis of silver-nanoparticles from Annona reticulata leaves aqueous extract and its mosquito larvicidal and anti-microbial activity on human pathogens. *Biotechnol. Rep.* **21**, e00297 (2019).
8. Yin, J. *et al*. A hydrogen peroxide electrochemical sensor based on silver nanoparticles decorated silicon nanowire arrays. *Electrochim. Acta* **56**, 3884–3889 (2011).
9. Kumar, B. *et al. In vitro* evaluation of silver nanoparticles cytotoxicity on Hepatic cancer (Hep-G2) cell line and their antioxidant activity: Green approach for fabrication and application. *J. Photochemistry Photobiology B: Biol.* **159**, 8–13 (2016).
10. Švecová, M., Ulbrich, P., Dendisová, M. & Matějka, P. SERS study of riboflavin on green-synthesized silver nanoparticles prepared by reduction using different flavonoids: What is the role of flavonoid used? *Spectrochimica Acta Part. A: Mol. Biomolecular Spectrosc.* **195**, 236–245 (2018).
11. Sathishkumar, P., Gu, F. L., Zhan, Q., Palvannan, T. & Yusoff, A. R. M. Flavonoids mediated 'Green'nanomaterials: A novel nanomedicine system to treat various diseases–Current trends and future perspective. *Mater. Lett.* **210**, 26–30 (2018).
12. Marslin, G. *et al*. Secondary metabolites in the green synthesis of metallic nanoparticles. *Mater.* **11**, 940 (2018).
13. Shah, M., Fawcett, D., Sharma, S., Tripathy, S. K. & Poinern, G. E. J. Green synthesis of metallic nanoparticles via biological entities. *Mater.* **8**, 7278–7308 (2015).
14. Parthibavarman, M., Bhuvaneshwari, S., Jayashree, M. & BoopathiRaja, R. Green Synthesis of Silver (Ag) Nanoparticles Using Extract of Apple and Grape and with Enhanced Visible Light Photocatalytic Activity. *BioNanoScience* **9**, 423–432 (2019).

15. Guan, Y. *et al*. AgNPs Modified Glass Carbon Electrode Prepared with Gelatin as an Additive for Hydrogen Peroxide Sensor. *Int. J. Electrochem. Sci.* **13**, 7696–7705 (2018).
16. Zhao, F., Zhou, M., Wang, L., Huang, Z. & Chu, Y. One-step voltammetric deposition of l-proline assisted silver nanoparticles modified glassy carbon electrode for electrochemical detection of hydrogen peroxide. *J. Electroanalytical Chem.* **833**, 205–212 (2019).
17. Dou, J. *et al*. Wall thickness-tunable AgNPs-NCNTs for hydrogen peroxide sensing and oxygen reduction reaction. *Electrochim. Acta* **306**, 466–476 (2019).
18. Yu, L. *et al*. Enhanced photoelectrochemical and sensing performance of novel TiO2 arrays to H2O2 detection. *Sens. Actuators B: Chem.* **211**, 111–115 (2015).
19. Luo, Y., Lu, W., Chang, G., Liao, F. & Sun, X. One-step preparation of Ag nanoparticle–decorated coordination polymer nanobelts and their application for enzymeless H2O2 detection. *Electrochim. Acta* **56**, 8371–8374 (2011).
20. Kumar, V. *et al*. Enhanced electron transfer mediated detection of hydrogen peroxide using a silver nanoparticle–reduced graphene oxide–polyaniline fabricated electrochemical sensor. *RSC Adv.* **8**, 619–631 (2018).
21. Qin, X. *et al*. Green photocatalytic synthesis of Ag nanoparticle-decorated TiO2 nanowires for nonenzymatic amperometric H2O2 detection. *Electrochim. Acta* **74**, 275–279 (2012).
22. Zhou, Y. & Tang, R.-C. Facile and eco-friendly fabrication of colored and bioactive silk materials using silver nanoparticles synthesized by two flavonoids. *Polym.* **10**, 404 (2018).
23. Vanaraj, S., Keerthana, B. B. & Preethi, K. Biosynthesis, Characterization of Silver Nanoparticles Using Quercetin from Clitoria ternateaL to Enhance Toxicity Against Bacterial Biofilm. *J. Inorg. Organomet. Polym. Mater.* **27**, 1412–1422 (2017).
24. Sun, W., Gao, Rf & Jiao, K. Electrochemistry and Electrocatalysis of a Nafion/Nano-CaCO3/Hb Film Modified Carbon Ionic Liquid Electrode Using BMIMPF6 as Binder. *Electroanalysis: An. Int. J. Devoted Fundamental Practical Asp. Electroanalysis* **19**, 1368–1374 (2007).
25. Yavari, M., Mazloum-Ardakani, M. & Khoshroo, A. Influence of Nitrogen Doping on the Electrocatalytic Effect of TiO2 Nanofibers. *J. Electrochem. Soc.* **164**, H903–H907 (2017).
26. Chai, L. *et al*. Chitosan, a new and environmental benign electrode binder for use with graphite anode in lithium-ion batteries. *Electrochim. Acta* **105**, 378–383 (2013).
27. Chen, H. *et al*. Direct electrochemistry and electrocatalysis of horseradish peroxidase immobilized in Nafion-RTIL composite film. *Electrochem. Commun.* **9**, 469–474 (2007).
28. Gholami, M. & Koivisto, B. A flexible and highly selective non-enzymatic H2O2 sensor based on silver nanoparticles embedded into Nafion. *Appl. Surf. Sci.* **467**, 112–118 (2019).
29. Wei, Y. & Ito, Y. Preparative isolation of imperatorin, oxypeucedanin and isoimperatorin from traditional Chinese herb "bai zhi" Angelica dahurica (Fisch. ex Hoffm) Benth. et Hook using multidimensional high-speed counter-current chromatography. *J. Chromatogr. A* **1115**, 112–117 (2006).
30. Ranjbar, S. *et al*. Studies of the interaction between isoimperatorin and human serum albumin by multispectroscopic method: identification of possible binding site of the compound using esterase activity of the protein. The Scientific World Journal 2013 (2013).
31. Meng-yue, W., Min-ru, J., Yu-ying, M. and Xiao-bo, L. Pharmacological Effect of Four Linear Furocoumarins in Radix Angelicae dahuricae. Natural Product Research & Development 22 (2010).
32. Shi, X. *et al*. Identification of *in vitro* and *in vivo* metabolites of isoimperatorin using liquid chromatography/mass spectrometry. *Food Chem.* **1**, 357–365 (2013).
33. Shokoohinia, Y., Hosseinzadeh, L., Moieni-Arya, M., Mostafaie, A. and Mohammadi-Motlagh, H.-R. Osthole attenuates doxorubicin-induced apoptosis in PC12 cells through inhibition of mitochondrial dysfunction and ROS production. BioMed research international 2014 (2014).
34. Shokoohinia, Y., Hosseinzadeh, L., Alipour, M., Mostafaie, A. and Mohammadi-Motlagh, H.-R. Comparative evaluation of cytotoxic and apoptogenic effects of several coumarins on human cancer cell lines: osthole induces apoptosis in p53-deficient H1299 cells. Advances in pharmacological sciences **2014** (2014).
35. Kang, J.-H., Lee, S.-K. & Yim, D.-S. Effect of isoimperatorin on the proliferation of prostate cancer cell line DU145 cells. *Biomolecules Therapeutics* **13**, 185–189 (2005).
36. Tan, N., Bilgin, M., Tan, E. & Miski, M. Antibacterial activities of pyrenylated coumarins from the roots of Prangos hulusii. *Molecules* **22**, 1098 (2017).
37. Guo, N. *et al*. *In vitro* activity of isoimperatorin, alone and in combination, against M ycobacterium tuberculosis. *Lett. Appl. microbiology* **58**, 344–349 (2014).
38. Chansaenpak, K., Kamkaew, A., Weeranantanapan, O., Suttisintong, K. & Tumcharern, G. Coumarin Probe for Selective Detection of Fluoride Ions in Aqueous Solution and Its Bioimaging in Live Cells. *Sens.* **18**, 2042 (2018).
39. Jin, L., Tan, X., Dai, L., Bai, H. & Wang, Q. Modulation of fluorescence sensing properties of coumarin-based fluorescent probe for H2S and its application in cell imaging. Spectrochimica Acta Part A: Molecular and Biomolecular Spectroscopy, **117187** (2019).
40. Kim, I., Kim, D., Sambasivan, S. & Ahn, K. H. Synthesis of π-Extended Coumarins and Evaluation of Their Precursors as Reactive Fluorescent Probes for Mercury Ions. Asian. *J. Org. Chem.* **1**, 60–64 (2012).
41. Starzak, K. *et al*. Fluorescence Quenching-Based Mechanism for Determination of Hypochlorite by Coumarin-Derived Sensors. *Int. J. Mol. Sci.* **20**, 281 (2019).
42. Wu, Q. *et al*. Coumarin amide derivatives as fluorescence chemosensors for cyanide anions. *Mater. Chem. Phys.* **161**, 43–48 (2015).
43. Sahu, N. *et al*. Synthesis of silver nanoparticles using flavonoids: hesperidin, naringin and diosmin, and their antibacterial effects and cytotoxicity. *Int. Nano Lett.* **6**, 173–181 (2016).
44. Osonga, F. J. *et al*. Flavonoid-derived anisotropic silver nanoparticles inhibit growth and change the expression of virulence genes in Escherichia coli SM10. *RSC Adv.* **8**, 4649–4661 (2018).
45. Reddy, N. J., Vali, D. N., Rani, M. & Rani, S. S. Evaluation of antioxidant, antibacterial and cytotoxic effects of green synthesized silver nanoparticles by Piper longum fruit. *Mater. Sci. Engineering: C.* **34**, 115–122 (2014).
46. Shankar, S. S., Rai, A., Ahmad, A. & Sastry, M. Rapid synthesis of Au, Ag, and bimetallic Au core–Ag shell nanoparticles using Neem (Azadirachta indica) leaf broth. *J. colloid interface Sci.* **275**, 496–502 (2004).
47. Fu, J. *et al*. A new polymorph of isoimperatorin. *Pharm. Dev. Technol.* **23**, 849–856 (2018).
48. Larkin, P. Infrared and Raman spectroscopy: principles and spectral interpretation. (Elsevier, 2017).
49. Jayaseelan, C., Ramkumar, R., Rahuman, A. A. & Perumal, P. Green synthesis of gold nanoparticles using seed aqueous extract of Abelmoschus esculentus and its antifungal activity. *Ind. Crop. Products* **45**, 423–429 (2013).
50. Raja, K., Saravanakumar, A. & Vijayakumar, R. Efficient synthesis of silver nanoparticles from Prosopis juliflora leaf extract and its antimicrobial activity using sewage. *Spectrochimica Acta Part. A: Mol. Biomolecular Spectrosc.* **97**, 490–494 (2012).
51. Mangalam, J., Kumar, M., Sharma, M. & Joshi, M. High adsorptivity and visible light assisted photocatalytic activity of silver/reduced graphene oxide (Ag/rGO) nanocomposite for wastewater treatment. *Nano-Structures Nano-Objects* **17**, 58–66 (2019).
52. Wood, S., Metcalf, D., Devine, D. & Robinson, C. Erythrosine is a potential photosensitizer for the photodynamic therapy of oral plaque biofilms. *J. Antimicrobial Chemotherapy* **57**, 680–684 (2006).
53. Roushani, M., Mavaei, M. & Rajabi, H. R. Graphene quantum dots as novel and green nano-materials for the visible-light-driven photocatalytic degradation of cationic dye. *J. Mol. Catal. A: Chem.* **409**, 102–109 (2015).

54. Silva, Z. S. Jr *et al*. Papain gel containing methylene blue for simultaneous caries removal and antimicrobial photoinactivation against Streptococcus mutans biofilms. *Sci. Rep.* **6**, 33270 (2016).
55. Silva, I. M. P., Byzynski, G., Ribeiro, C. & Longo, E. Different dye degradation mechanisms for ZnO and ZnO doped with N (ZnO: N). *J. Mol. Catal. A: Chem.* **417**, 89–100 (2016).
56. Theurich, J., Lindner, M. & Bahnemann, D. Photocatalytic degradation of 4-chlorophenol in aerated aqueous titanium dioxide suspensions: a kinetic and mechanistic study. *Langmuir* **12**, 6368–6376 (1996).
57. Li, X., Cubbage, J. W., Tetzlaff, T. A. & Jenks, W. S. Photocatalytic degradation of 4-chlorophenol. 1. The hydroquinone pathway. *J. Org. Chem.* **64**, 8509–8524 (1999).
58. Pera-Titus, M., García-Molina, V., Baños, M. A., Giménez, J. & Esplugas, S. Degradation of chlorophenols by means of advanced oxidation processes: a general review. Applied. *Catal. B: Environ.* **47**, 219–256 (2004).
59. Descorme, C. Catalytic wastewater treatment: oxidation and reduction processes. Recent studies on chlorophenols. *Catal. Today* **297**, 324–334 (2017).
60. Mills, A. & Wang, J. *Photomineralisation 4-chlorophenol sensitised TiO2 thin films. J. Photochemistry Photobiology A: Chem.* **118**, 53–63 (1998).
61. Satuf, M. L., Brandi, R. J., Cassano, A. E. & Alfano, O. M. Photocatalytic degradation of 4-chlorophenol: a kinetic study. *Appl. Catal. B: Environ.* **82**, 37–49 (2008).
62. Aragon, A. G. *et al*. Synthesis and application of N-doped TiO2/CdS/poly (1, 8-diaminocarbazole) composite for photocatalytic degradation of 4-chlorophenol under visible light. *Electrochim. Acta* **314**, 73–80 (2019).
63. Karyakin, A. A. *et al*. Prussian blue based nanoelectrode arrays for H2O2 detection. *Anal. Chem.* **76**, 474–478 (2004).
64. Xie, F., Cao, X., Qu, F., Asiri, A. M. & Sun, X. Cobalt nitride nanowire array as an efficient electrochemical sensor for glucose and H2O2 detection. *Sens. Actuators B: Chem.* **255**, 1254–1261 (2018).
65. Chen, D. *et al*. Preparation of highly sensitive Pt nanoparticles-carbon quantum dots/ionic liquid functionalized graphene oxide nanocomposites and application for H2O2 detection. *Sens. Actuators B: Chem.* **255**, 1500–1506 (2018).
66. Sun, Y. *et al*. Graphene/intermetallic PtPb nanoplates composites for boosting electrochemical detection of H2O2 released from cells. *Anal. Chem.* **89**, 3761–3767 (2017).
67. Kurowska, E., Brzózka, A., Jarosz, M., Sulka, G. & Jaskuła, M. Silver nanowire array sensor for sensitive and rapid detection of H2O2. *Electrochim. Acta* **104**, 439–447 (2013).
68. Nia, P. M., Lorestani, F., Meng, W. P. & Alias, Y. A novel non-enzymatic H2O2 sensor based on polypyrrole nanofibers–silver nanoparticles decorated reduced graphene oxide nano composites. *Appl. Surf. Sci.* **332**, 648–656 (2015).
69. Wang, Q.-M., Niu, H.-L., Mao, C.-J., Song, J.-M. & Zhang, S.-Y. Facile synthesis of trilaminar core-shell Ag@ C@ Ag nanospheres and their application for H2O2 detection. *Electrochim. Acta* **127**, 349–354 (2014).
70. Miao, X., Yang, C., Leung, C.-H. & Ma, D.-L. Application of iridium (III) complex in label-free and non-enzymatic electrochemical detection of hydrogen peroxide based on a novel "on-off-on" switch platform. *Sci. Rep.* **6**, 25774 (2016).
71. Zhang, L., Zhai, Y., Gao, N., Wen, D. & Dong, S. Sensing H2O2 with layer-by-layer assembled Fe3O4–PDDA nanocomposite film. *Electrochem. Commun.* **10**, 1524–1526 (2008).
72. Yang, L., Xu, C., Ye, W. & Liu, W. An electrochemical sensor for H2O2 based on a new Co-metal-organic framework modified electrode. *Sens. Actuators B: Chem.* **215**, 489–496 (2015).
73. Chahardoli, A., Karimi, N. & Fattahi, A. Nigella arvensis leaf extract mediated green synthesis of silver nanoparticles: Their characteristic properties and biological efficacy. *Adv. Powder Technol.* **29**, 202–210 (2018).
74. Ahmadi, F., Shokoohinia, Y., Javaheri, S. & Azizian, H. Proposed binding mechanism of galbanic acid extracted from Ferula assa–foetida to DNA. *J. Photochemistry Photobiology B: Biol.* **166**, 63–73 (2017).
75. Shokoohinia, Y., Sajjadi, S.-E., Gholamzadeh, S., Fattahi, A. & Behbahani, M. Antiviral and cytotoxic evaluation of coumarins from Prangos ferulacea. *Pharm. Biol.* **52**, 1543–1549 (2014).
76. Roy, K., Sarkar, C. & Ghosh, C. Photocatalytic activity of biogenic silver nanoparticles synthesized using yeast (Saccharomyces cerevisiae) extract. *Appl. Nanosci.* **5**, 953–959 (2015).

Acknowledgements

The authors gratefully acknowledge the Research Council of Kermanshah University of Medical Sciences for financial support.

Author contributions

Maryamosadat Mavaei did the catalytic studies. Yalda Shookohinia did the herbal part; the isolation and purification of isoimperatorin. Azam Chahardoli synthesized nanoparticles. and Alireza Khoshroo assisted in the electrochemical investigation. All the authors took part in writing and editing the manuscript. Ali Fattahi edited the manuscript, prepared materials, designed experiments.

Competing interests

The authors declare no competing interests.

Additional information

Correspondence and requests for materials should be addressed to A.F.

Reprints and permissions information is available at www.nature.com/reprints.

Publisher's note Springer Nature remains neutral with regard to jurisdictional claims in published maps and institutional affiliations.